Geophysical Research Letters

RESEARCH LETTER
10.1029/2019GL086649

Submesoscale Fronts in the Antarctic Marginal Ice Zone and Their Response to Wind Forcing

Sebastiaan Swart[1,2], Marcel D. du Plessis[2,3], Andrew F. Thompson[4], Louise C. Biddle[1], Isabelle Giddy[1,2], Torsten Linders[1], Martin Mohrmann[1], and Sarah-Anne Nicholson[3]

[1]Department of Marine Sciences, University of Gothenburg, Gothenburg, Sweden, [2]Department of Oceanography, University of Cape Town, Rondebosch, South Africa, [3]Southern Ocean Carbon-Climate Observatory (SOCCO), CSIR, Cape Town, South Africa, [4]Environmental Science and Engineering, California Institute of Technology, Pasadena, CA, USA

Key Points:
- Using combined surface and underwater robotic observations, we observe haline-dominated submesoscale fronts in the Antarctic MIZ
- Enhanced wind speeds reduce the magnitude of lateral submesoscale fronts within the surface mixed layer
- Submesoscale wind-front interactions cause a continuous interplay between front slumping and vertical mixing, arresting lateral shear

Supporting Information:
- Supporting Information SI

Correspondence to:
S. Swart,
sebastiaan.swart@marine.gu.se

Citation:
Swart, S., du Plessis, M. D., Thompson, A. F., Biddle, L. C., Giddy, I., Linders, T., et al. (2020). Submesoscale fronts in the Antarctic marginal ice zone and their response to wind forcing. *Geophysical Research Letters*, *47*, e2019GL086649. https://doi.org/10.1029/2019GL086649

Received 13 DEC 2019
Accepted 2 MAR 2020
Accepted article online 4 MAR 2020

Abstract Submesoscale flows in the ocean are energetic motions, O(1–10 km), that influence stratification and the distributions of properties, such as heat and carbon. They are believed to play an important role in sea-ice-impacted oceans by modulating air-sea-ice fluxes and sea-ice extent. The intensity of these flows and their response to wind forcing are unobserved in the sea-ice regions of the Southern Ocean. We present the first submesoscale-resolving observations in the Antarctic marginal ice zone (MIZ) collected by surface and underwater autonomous vehicles, for >3 months in austral summer. We observe salinity-dominated lateral density fronts occurring at sub-kilometer scales. Surface winds are shown to modify the magnitude of the mixed-layer density fronts, revealing strongly coupled atmosphere-ocean processes. We posture that these wind-front interactions occur as a continuous interplay between front slumping and vertical mixing, which leads to the dispersion of submesoscale fronts. Such processes are expected to be ubiquitous in the Southern Ocean MIZ.

Plain Language Summary Satellite radar imagery shows evidence of 1–10 km eddies and jets in the ocean adjacent to the sea-ice edge around Antarctica. We use field observations of temperature, salinity, and wind speed from autonomous robotic platforms deployed in the sea-ice zone for >3 months. These measurements provide estimates of the surface ocean density fronts which are controlled primarily by lateral variations in salinity. We show that, during high wind speeds, these surface fronts temporarily dissipate, indicating an atmosphere-ocean coupling occurring at the submesoscale. The fronts strengthen again during low wind speed, which is thought to be because the stirring of the fresher surface layer by mesoscale eddies leads to the generation of the submesoscale fronts. Providing in situ observations of such features improves our understanding of the small-scale ocean and climate processes at play, such as how heat and carbon may exchange between the atmosphere and the ocean.

1. Introduction

The sea-ice-impacted ocean around Antarctica is vast, with annual sea-ice growth and melt occurring over approximately 18 $\times 10^6$ km^2—equivalent to the surface area of South America. Southern Ocean air-sea-ice fluxes impact the ocean heat and carbon budget (e.g., Marshall & Zanna, 2014), water mass transformation (Walin, 1982), the global overturning circulation (Abernathey et al., 2016), sea-ice distribution, and numerous biogeochemical processes. Despite this, atmosphere-ocean physical processes within the Marginal Ice Zone (MIZ) are poorly understood due to the paucity of *in situ* observations brought about by its seasonal ice cap and remoteness. Ongoing efforts (e.g., under-ice profiling floats and seal tag data) are helping to address this data gap, albeit at relatively coarse temporal and spatial resolution (e.g., Campbell et al., 2019; Pellichero et al., 2017). Current observational efforts remain unable to resolve the rapidly evolving dynamics of the surface layer ocean in the MIZ. This contributes to both a poor mechanistic understanding and to uncertainty in modeling the impact of ocean-ice-atmosphere processes on larger-scale climate.

In addition to surface mechanical and buoyancy forcing, the formation and evolution of lateral density gradients, or fronts, may also significantly impact upper ocean stratification. These fronts can become unstable to instabilities that form mixed layer eddies (Boccaletti et al., 2007; Thomas & Ferrari, 2008), which evolve rapidly (in the order of hours – days and at small lateral scales, O(1 km); Thomas et al., 2008), otherwise known as submesoscale flows (Rossby numbers of O(1)). When these flows become baroclinically

unstable, they slump and can generate rapid restratification in the mixed layer (Hosegood et al., 2006). Winds blowing over mixed-layer fronts can aid and destroy vertical stratification, depending on their orientation (du Plessis et al., 2019; Mahadevan et al., 2010; Thomas & Lee, 2005). In the MIZ, the surface layer is expected to contain energetic submesoscale processes given the potential for strong lateral gradients fed by seasonal sea-ice-induced freshwater fluxes (sea-ice melt and formation, such as those observed in the Arctic; Timmermans et al., 2008), while the presence of a freshwater lens will act to suppress submesoscale flows from forming in shallow mixed layers (reduction in the frontal potential energy). Alternatively, submesoscale flows, whether intermittent or quasi-permanent, are likely to generate vertical fluxes of heat and salt (Thomas et al., 2008) that will alter the buoyancy and heat budget of the upper ocean, further adjusting sea-ice melt and formation rates. This is especially relevant in the Antarctic MIZ, where warm and salty Circumpolar Deep Water (CDW) lies closely under the surface mixed layer.

Although submesoscale fronts are considered to be ubiquitous in the surface ocean (e.g., Adams et al., 2019; Johnson et al., 2016; Ramachandran et al., 2018; Thomas et al., 2013), until now, we have no observations at the required scale to assess their prevalence and strength in the Antarctic MIZ. This is especially true at seasonal scales that capture sea-ice formation or melting processes and their associated impact on the upper ocean physics and biogeochemistry. Most of our understanding of submesoscale processes in the sea-ice polar regions exists from theoretical estimates and modeling simulations (Horvat et al., 2016; Lu et al., 2015; Manucharyan & Thompson, 2017) and a handful of observational efforts limited to the Arctic (Lu et al., 2015; Timmermans et al., 2008, Timmermans & Winsor, 2013; Toole et al., 2010; von Appen et al., 2018). In the Antarctic, sea-ice extends to considerably lower latitudes (55°S) compared with the Arctic and is exposed to stronger surface forcing, related to storms located in the westerly wind belt, as well as a more energetic surface circulation, associated with the Antarctic Circumpolar Current and northern limbs of the polar gyres. This means that lessons learned from the Arctic may not immediately translate to Southern Ocean conditions. To our knowledge, multiscale (fine spatial scale to multi-month temporal scale) observations have not previously been reported from the Southern Ocean MIZ.

The field site of the Robotic Observations and Modeling of the MIZ (ROAM-MIZ) project represents a nexus for active surface wind forcing and enhanced vertical and lateral property gradients in the upper ocean brought on primarily by sea-ice formation and melt processes (e.g., Pellichero et al., 2017), which gives rise to lateral gradients in density. Strong time-mean wind stress, where a band of maximum wind force (Lin et al., 2018) induced by transient storms (> 20 m s^{-1}; Yuan, 2004), characterizes our study region. These storms add a time-varying and rotational component to the background wind forcing, which interacts directly with lateral density ocean gradients (du Plessis et al., 2019) driven mostly by seasonal freshwater fluxes (varying buoyancy flux; e.g., Massom & Stammerjohn, 2010). We see evidence for these density gradients and associated instabilities occurring in the MIZ from high-resolution Sentinel-SAR imagery (Figure 1a), where signatures of 5- to 10-km-scale ocean eddies and filaments are apparent in the sea ice (Manucharyan & Thompson, 2017). We hypothesize that following the sea-ice melt, freshwater anomalies are stirred by mesoscale motions that generate haline-dominated fronts through frontogenesis. These fronts store potential energy that can promote submesoscale flows. Furthermore, the intense surface winds of the Southern Ocean interact with these fine-scale fronts at synoptic time scales, providing vertical shear that can destroy vertical stratification and impact the intensity of submesoscale fronts.

We present high-resolution in situ observations (0.2- to 120-km resolution between December 2018 and March 2019) obtained in the Southern Ocean MIZ from an autonomous surface vehicle, a Sailbuoy, paired with a profiling Seaglider. With these observations, we show that submesoscale fronts persist into late summer, but their intensity responds rapidly to intermittent wind forcing. We expect such atmosphere-ocean interactions to be ubiquitous in both the Southern Ocean and Arctic MIZs.

2. Data and Methods

Robotic surveys were conducted in recently formed open waters, approximately 100 km from the rapidly retreating sea-ice edge (Figure 1b) at 60°S, 0°E. At the experiment location, satellite data depict the sea-ice present ~4 days before deployment (Figure 1c) and then rapidly retreating ~700 km southwards in a week. An autonomous surface vehicle, the Offshore Sensing Sailbuoy (2-m length, 60-kg displacement), collected surface temperature (T), salinity (S), and meteorological measurements. The Sailbuoy is wind propelled,

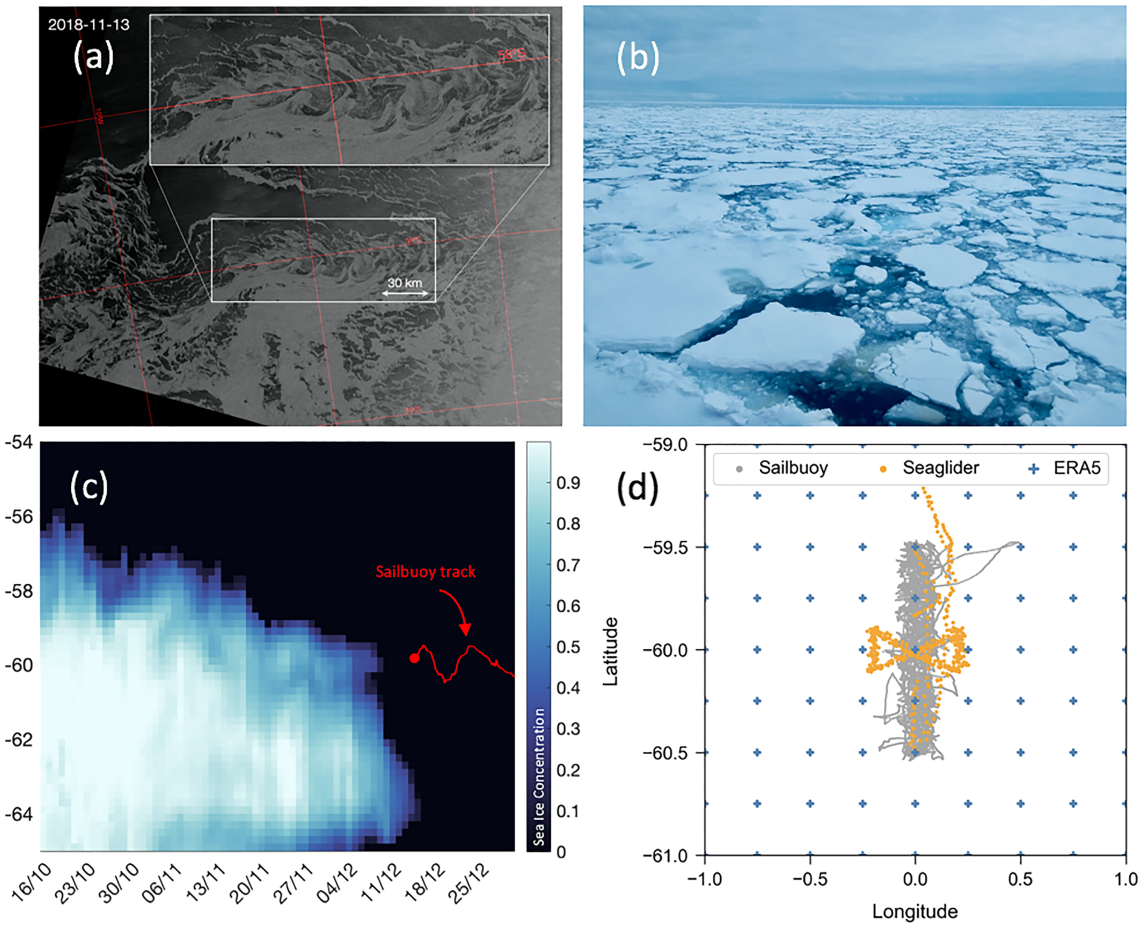

Figure 1. (a) Sentinel-1 synthetic aperture radar image from 13 November 2018 (1 month prior to robotic deployments) suggesting ocean submesoscale features present at the sea-ice margins of O(5–10 km). (b) Photo taken from the SA Agulhas II (15 December 2018; 61.07°S, 0.05°E) showing sea-ice conditions ~100 km south of the study location. (c) Hövmöller of the sea-ice concentration from combined AMSR2 and SSMI data centered on 0°E (the red dot and line shows the deployment and initial track of the Sailbuoy). (d) Seaglider and Sailbuoy locations during the study. Crosses denote the ERA5 reanalysis winds grid, as in Figure S1.

with solar panels powering scientific sensors and navigation systems, enabling it to remain at sea for months (Ghani et al., 2014). During the deployment, between 15 December 2018 and 1 March 2019, the Sailbuoy maintained a north-south transect of 112 km in length (Figure 1d), achieving 17 (O(100 km)) transects repeated every 4.1 ± 1.8 days. An Aanderaa 4319 conductivity and temperature sensor was installed at 0.5-m depth in a flow through keel-bulb that sampled every 30 s. Data were averaged in 10-min bins and transmitted back to shore. Future observational efforts should seek even higher sampling frequency to account for rapidly changing properties over space and time. Antifouling coating was applied to the platform and bulb with no biofouling evident on recovery and no sensor drift recorded when compared to conductivity-temperature-depth (CTD) measurements from collocated glider and ship thermosalinograph measurements.

An Airmar WX-200 Ultrasonic Weather Station was mounted on a mast 0.7 m above sea level measuring true wind speed, wind gust (maximum wind speed every 10 min) and direction, barometric pressure, and air temperature. The instrument is designed for moving platforms, with the ability to dynamically correct winds using an internal compass and correct up to a 30° pitch in rough seas. The sensor sampled at 1 Hz and then averaged the data in 10-min bins, before transmitting data back to shore. Details on sensor accuracy and behavior in variable weather conditions, as well as referencing the surface winds to 10 m above sea level, can be found in Schmidt et al. (2017). On 8 February 2019, we lost functionality of the Airmar sensor due to unknown damage (suspected iceberg collision) to the vehicle during the mission. To extend the wind speed time series and collocate wind observations with the glider data, we use gridded wind reanalysis

products. ERA5, NCEP, and CFS reanalysis winds are compared to in situ Sailbuoy winds, which shows that CSF and ERA5 are comparable and better than NCEP. We thus use ERA5 winds in this study ($r = 0.75$; RMSE = 2.09 m s^{-1}; Figure S1 of the supporting information). This result is supported by Schmidt et al. (2017) using wind speed measurements from multiple Wave Gliders in the Southern Ocean.

Hydrographic data were collected by a Seaglider, profiling to 1,000 m, over the central domain of the Sailbuoy transect from 15 December 2018 and 26 March 2019 (101 days). The glider was placed in a repeat "bow-tie" sampling pattern with lateral length-scale transects of 22 km (Figure 1d) and on two occasions completed a 100-km north-south transect to resolve the local mesoscale (O(100 km)) gradient. The CTD sampled nominally at 0.2 Hz and the data were quality controlled against ship CTD profiles (as in Swart et al., 2015), as well as applying the most up-to-date conductively thermal lag corrections based on the glider flight model to estimate conductivity cell flow through rates (C. Eriksen, unpublished). Only observations between the surface and until 15 m above the mixed layer depth (MLD) are used to compute mixed layer gradients in order to avoid internal wave processes or larger conductivity thermal lag errors nearer the pycnocline. By utilizing the upper part of the glider "saw-tooth" pattern (successive climb and dive profiles; Figure S2a), we are able to resolve surface-layer lateral density gradients at resolutions of between 10 and 200 m and ~20 min, (median lateral spacing ~120 m between 0- and 50-m depth; Figures S2b and S2c). This high-resolution "snapshot" sampling of the lateral density gradient is repeated at each glider dive interval, which is approximately 4 hourly. ERA5 wind speed data are collocated at the location and time of the glider throughout the deployment.

3. Results and Discussion

3.1. Surface-Layer Gradients and Their Scale Sensitivity

Sailbuoy surface T and S sampling obtained an average resolution of 0.49 ± 0.23 km, thus resolving length scales of O(1 km), enabling observations of submesoscale lateral fronts and features. An internal Rossby radius, (Lr = NH/f, where N is the buoyancy frequency in the mixed layer, H is the MLD, which was 41 ± 8.6 m during the survey, as determined using the density criteria, $\rho = 0.03$ kg m^{-3}, and $f \approx 1.2 \times 10^{-4}$ s^{-1} is the Coriolis frequency) provides the length scale for submesoscale flows to develop in the surface layer (Boccaletti et al., 2007). During our survey period, Lr = 2.0 ± 0.5 km was obtained from the glider survey, suggesting the applicability of the autonomous platforms to sample at scales smaller than Lr.

We find lateral density gradients existing at all observed scales (sub-kilometer to 100 km scales; Figures 2a and 3; note that in Figure 2, T and S are scaled according to their respective contributions to changes in density). Lateral changes in density are dominated by S variations, compared with only minor contributions from changes in T. The relative contribution of T and S gradients to lateral density fronts is further estimated using the lateral density ratio, $R = \alpha\Delta T/\Delta S$, where α and β are the thermal expansion and haline contraction coefficients, respectively, and ΔT and ΔS are the lateral temperature and salinity gradients, respectively. $R = 1$ would infer full compensation, while deviations from 1 represent uncompensated fronts by either temperature ($R > 1$) or salinity ($0 < R < 1$) (Rudnick & Ferrari, 1999). $R < 0$ indicates conditions where fronts are reinforced by temperature gradients working in concert with salinity gradients. The high-resolution data show that lateral T and S gradients are noncompensating and S variations dominate the density gradients ($R < 1$) with the histogram peaking at $R \sim 0$ (Figure 2c). This contrasts the midlatitude regions, where T dominates uncompensated density fronts (Hosegood et al., 2006; Johnson et al., 2012). Separating the analysis between early summer and late summer shows a flattening and small deviation in the distribution of R towards −1, over the 3-month time series (Figure 2c). This indicates an increasing role of T towards reinforcing density fronts due to seasonal warming and a reduction in the strength of the S contribution to the density gradient of the fronts, potentially by slow mixing processes or entrainment (the low saline mixed-layer waters from the early summer sea-ice melt are mixed with saltier CDW from below). However, the solar heating of the mixed layer in summer (0–190 W m^{-2} during this study) is not enough to significantly adjust R towards T control of the surface density gradients. Nonetheless, strong salinity-driven fronts continue to occur with time (Figure 2a), indicating that mixing processes do not significantly reduce surface ocean density gradients (similar to Chukchi Sea observations by Timmermans & Winsor, 2013) and that the stirring of waters with varying salinity continue long after the sea ice has retreated. We speculate that a supply of

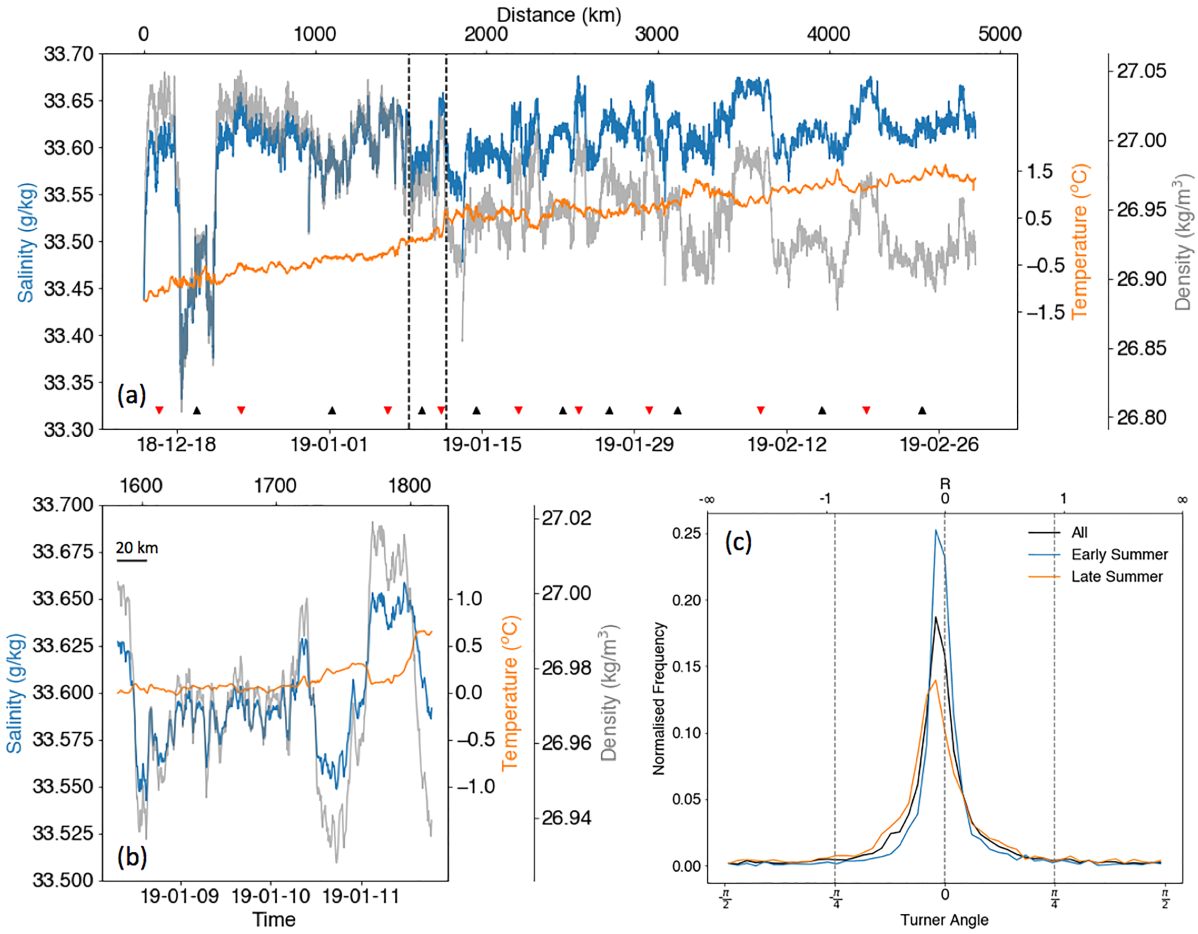

Figure 2. (a) Continuous surface temperature (T), salinity (S), and density measurements by the Sailbuoy over ~2.5 months. Red (black) triangle markers represent the start of Sailbuoy transects heading southward (northward). The dashed lines indicate an expanded view in (b) of T, S and density gradients at ~200-km scale. T and S ranges are proportionally scaled by the thermal expansion (α) and haline contraction (β) coefficients, so that equal displacements have equal effect on density. (c) Distributions of the density ratio, R, and Turner angle calculated from the Sailbuoy surface data for early summer (blue), late summer (orange), and the entire deployment (black).

freshwater is advected from more southern latitudes over time, where sea-ice melt extends further into the summer season.

The variations in the haline fronts (<1 km) observed by the Sailbuoy can exceed 0.5 g kg^{-1} km^{-1} with the 50th percentile = 0.03 g kg^{-1} km^{-1} and 95th percentile = 0.141 g kg^{-1} km^{-1} (Figure 2b). The lateral salinity gradients obtained only between consecutive glider up-cast and down-cast data (see section 2; Figure S2) indicate comparable, strong salinity fronts within the mixed layer (50th percentile = 0.025 g kg^{-1} km^{-1} and 95th percentile = 0.241 g kg^{-1} km^{-1}). The small, yet potentially important remains of thermal lag error in the salinity data within the mixed layer, between successive Seaglider climb and dive profiles (0.01 ± 0.02 g kg^{-1} km^{-1}), can lead to lateral salinity gradients being overestimated by ~15 ± 31%. This is an upper bound overestimate given that the salinity differences between profiles include actual lateral salinity fronts too.

Furthermore, wavenumber spectra are used to show the variance in the lateral density measured by the Sailbuoy over wavelengths of 1–50 km (Figure 3b). The surface density was first linearly interpolated to 400 m, the average distance between sampling, detrended, and smoothed with a 2 km Gaussian window before the power density spectra was computed. The best-fit wavenumber (k) slope for the surface density is $k \sim -2.4$ (Figure 3b). The fairly less steep wavenumber spectra found in this study indicate somewhat more energetic small-scale structures compared with those observed in the Arctic at 70°N ($k = -2.8$ from Timmermans & Winsor, 2013) and under Arctic sea ice (Timmermans et al., 2012) where spectra slopes

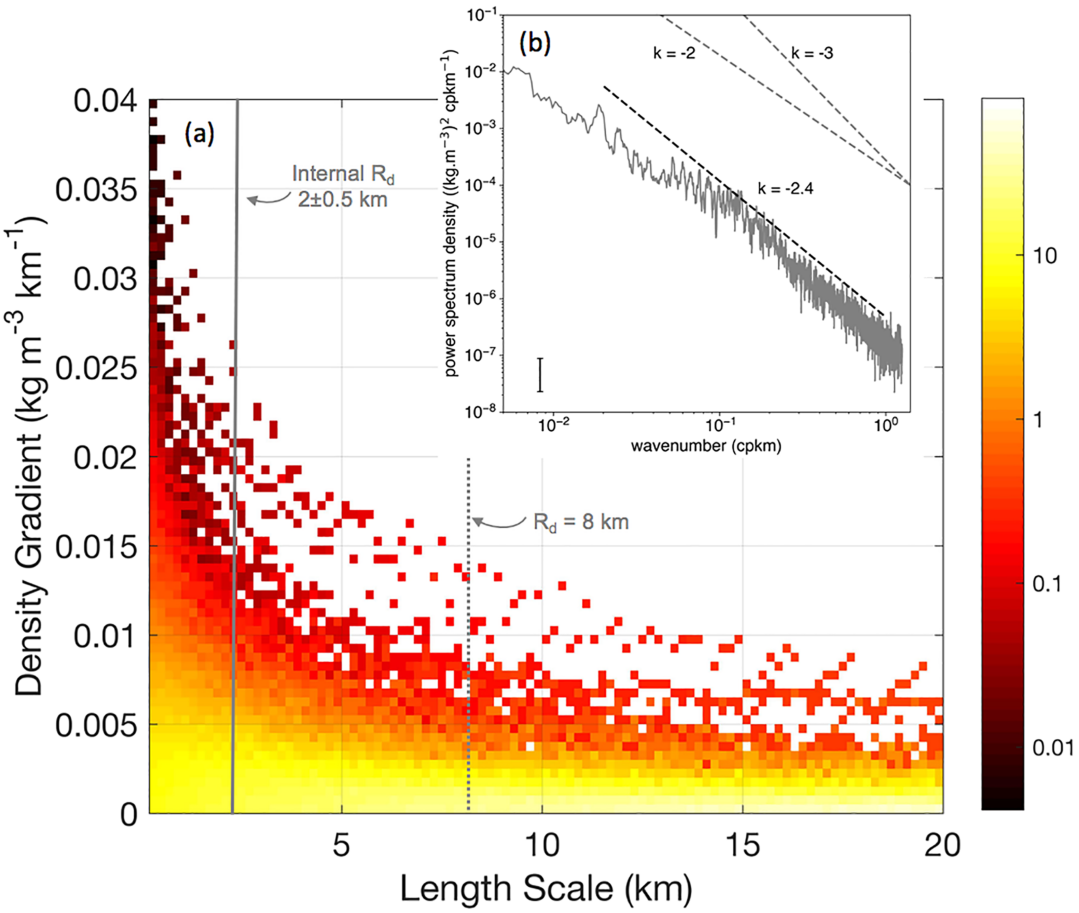

Figure 3. (a) Distribution of surface density gradients (kg m^{-3} km^{-1}) as sampled by different horizontal length scales (0.2 to 20 km). The log color scale represents the percentage count of the gradients at various scales. The internal and full-depth Rossby deformation radius for the study region are indicated. (b) Horizontal wavenumber spectra of the surface density variance from the Sailbuoy dataset. Dashed black line is the best-fit slope of −2.4 between 1 and 50 km. For reference, k^{-2} and k^{-3} slopes are indicated with gray dashed lines. The 95% confidence interval is shown.

were closer to k^{-3}. Overall, the in situ observations confirm the evidence of these active submesoscale flows seen in the SAR imagery (Figure 1a) adjacent to and extending ~100 km into the sea ice.

To assess the scale sensitivity of the fronts, continuous time series of surface density are subsampled between 0.2 and 30 km (Figure 3). The highest-resolution sampling (mean = 0.46 ± 0.23 km) reveals a spread of density gradients reaching up to 0.06 kg m^{-3} km^{-1} (equivalent lateral buoyancy gradient = 6×10^{-7} s^{-2}, hereafter reported as a lateral density gradient). These density gradients are lower bound estimates given that the surface fronts were unlikely to have been sampled perpendicularly by the Sailbuoy. By assessing the difference between the glider dive direction and the estimated front direction, we estimate that the glider (and comparatively for the Sailbuoy) underestimate the true lateral buoyancy gradient by 51% on average (similarly, this is computed to be 64% and 71% for glider observations by du Plessis et al., 2019, and Thompson et al., 2016, respectively). Once the sampling length scale is increased incrementally, there is a sharp drop off in density gradients, which converge between the internal and full-depth Rossby radius of deformation at this latitude ($R_{d\_internal}$ = 2 km, R_d = 8 km; Figure 2c). As a case in point, if one were to measure the surface thermohaline gradients in this region at length scales greater than 8 km, one would only observe density gradients of less than 0.01 kg m^{-3} km^{-1}, with the vast majority (63%) sampled at <0.005 kg m^{-3} km^{-1}. This emphasizes the need to sample at high spatial resolutions (<1 km) to capture the full surface variance in density at high latitudes, particularly in relatively shallow mixed layer environments (leading to smaller $R_{d\_internal}$) where sea-ice-induced freshwater layers can prevail (e.g., in the Arctic—Wulff et al., 2016).

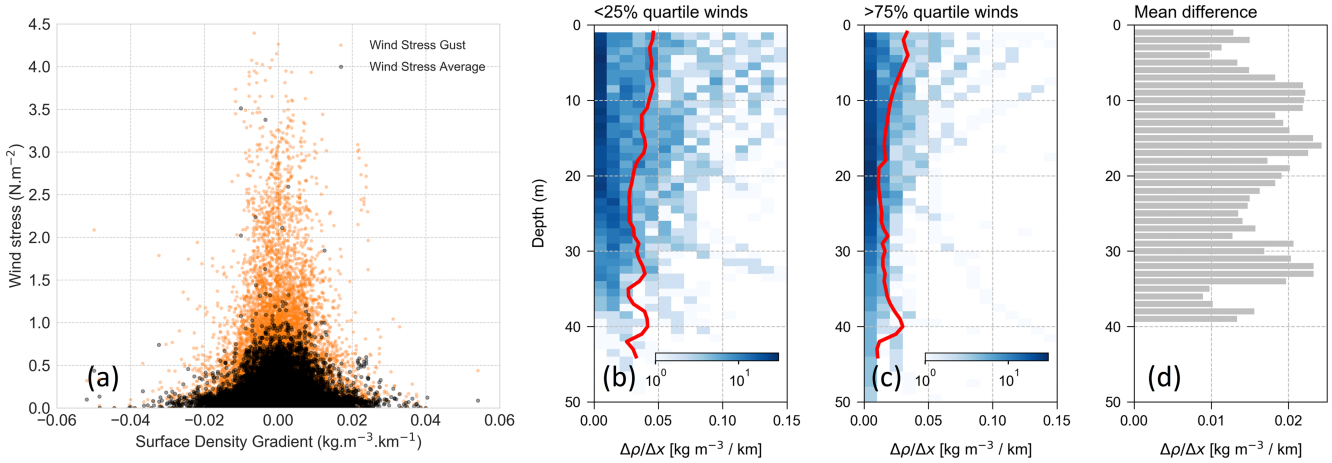

Figure 4. (a) Relation between surface lateral density gradients and wind stress (?) during the 2.5-month Sailbuoy deployment. Instantaneous 10-min wind gust stress is shown using gray dots. Seaglider measured lateral density gradients with depth at (b) low wind speeds (lower quartile) and (c) high wind speeds (upper quartile). The mean distribution of the gradients with depth are depicted by the red lines for each quartile. (d) The difference between the mean lateral density gradients for the high and low wind speed quartiles.

The heterogeneity in surface salinity ~4 days after the sea ice has melted from this location (Figure 1c) suggests that the open ocean near the sea-ice edge is almost immediately susceptible to lateral density gradients. These fronts have the potential to tilt from the vertical to the lateral and provide a restratifying buoyancy flux to the upper ocean over and above the existing buoyant freshwater layers associated with the recent sea-ice melt. Calculations of the vertical buoyancy flux associated with submesoscale mixed layer eddies (Boccaletti et al., 2007) from the glider data in this study show intermittent (weekly) periods of equivalent heat fluxes reaching up to 200 W m^{-2} (lower bound estimates given nonperpendicular transect of the buoyancy fronts by the glider). These equivalent heat fluxes, albeit intermittent, are of similar magnitude or larger than the solar heat flux received in this region during summer.

3.2. Surface-Layer Density Fronts Modified by Surface Winds

The paired Sailbuoy and Seaglider platforms provide high-resolution T and S data and concomitant wind speed measurements that allow us to assess the relationship between the fine-scale lateral gradients and wind. Interestingly, we observe a strong wind-front relationship in the study region, with higher wind stress resulting in a suppression of the stronger density gradients (Figure 4a). Sailbuoy data show that the largest density gradients (0.02–0.04 kg m^{-3} km^{-1}) decrease sharply at wind stress greater than ~0.3 N m^{-2}. Binning the data in 0.05 N m^{-2} intervals of wind stress reveals a sharp decrease in the density gradients at wind stress >0.4 N m^{-2}, while a Pearson correlation of $r = -0.77$ ($p \ll 0.01$) between the wind stress and density gradients underpins this as evidence for a coupled wind-front relationship.

A similar relationship is apparent from glider observations (upper 50 m; Figure S2), where the magnitude of submesoscale fronts separate out between the upper and lower quartiles of collocated ERA5 wind speeds (Figures 4b and 4c). High wind events (>75th percentile; 12.7 ± 2.6 m s^{-1}) are able to reduce lateral density gradients throughout the mixed layer by an average of 0.01 kg m^{-3} km^{-1} or reduce the median lateral fronts by 47 ± 12% compared with the quiescent wind phases (<25th percentile; 4.4 ± 1.2 m s^{-1}). This apparent wind-front interaction is consistent in the upper 40 m of the ocean with a slight decrease in the difference in the lateral gradients with depth (Figure 4d).

A plausible mechanism for these wind-front interactions, at the submesoscale, is termed thermohaline shear dispersion (first introduced in atmospheric studies by Moran & Pielke, 1994; and in high-resolution ocean simulations by Ferrari et al., 2001). To explain this mechanism, we pose that, in the Antarctic MIZ, energetic lateral density fronts dominated by salinity gradients slump under the action of baroclinic instability (e.g., Boccaletti et al., 2007; Fox-Kemper et al., 2008). Passing storms, and their associated higher wind forcing, enhance vertical shear stresses between the recently slumped surface layer and the layer below, driving shear-driven mixing by inertial oscillations that weaken the lateral density gradients in the upper ocean.

At these latitudes, inertial oscillations have a period of ~13 hr and a width of O(1 km), depending on the current velocity. In fairly shallow MIZ mixed layers (~40 m), the inertial oscillations will generate strong lateral currents and shear that can dissipate the lateral density fronts. Following the storm events, submesoscale fronts are thought to regenerate by the stirring of the fresher surface layer by mesoscale eddies. The modification of these fronts by stronger wind stress suggests that storm-driven mixing ultimately diffuses the submesoscale fronts by dispersion.

Our study region, and more broadly the Antarctic MIZ, is likely prone to such processes given that seasonal freshwater inputs by melting sea-ice result in strongly uncompensated fronts (Figure 2c), particularly given that the shear dispersion strength increases as the lateral buoyancy gradient squared (compensated fronts are balanced and thereby do not experience shear dispersion; Ferrari et al., 2001) and because of the strong wind forcing occurring in the Southern Ocean. How these processes are moderated in ice-covered oceans is yet to be observed and understood. However, the literature shows that lateral buoyancy gradients (and associated submesoscale fluxes) are present under Arctic sea ice (Timmermans et al., 2012) and so ice-induced shear stresses to the surface layer are likely to result in shear dispersion being active in ice-covered oceans.

4. Discussion and Summary

Following the rapid retreat of the Antarctic sea ice in early summer, in situ observations reveal lateral density fronts characterized by submesoscale salinity variations persisting to late summer. Resolving these surface-layer submesoscale fronts require sampling at sub-kilometer lateral scales and sub-daily temporal scales accounting for the rapidly-evolving effects of surface forcing (synoptic to seasonal variations in wind stress). Despite the suppression of submesoscale fronts by winds, they are not dissipated over the 3 months. This contrasts to the Bay of Bengal, where strong atmospheric forcing can adjust the basin-wide submesoscale gradients (Shroyer et al., 2019).

We expect these wind-front interactions to be ubiquitous over regions of large surface seasonal freshwater fluxes and strong surface winds such as the Southern Ocean MIZ. Resolving such fine-scale processes and associated submesoscale-induced vertical velocities (Klein & Lapeyre, 2009) are likely to have implications for accurately determining air-sea and air-sea-ice physical and biogeochemical fluxes (Swart et al., 2019). Current global climate model simulations show a large sensitivity to the magnitude and variability of vertical biophysical fluxes in the Southern Ocean (IPCC AR5). Therefore, subgrid scale processes are required to be parameterized correctly (Fox-Kemper et al., 2008) or otherwise represented directly in numerical simulations (Gruber et al., 2019). Future projections of the intensified and southward shifting westerly winds (positive Southern Annular Mode phase; Marshal, 2003) may have implications for submesoscale processes in the MIZ. This work suggests intensified winds are likely to reduce the lateral gradients associated with submesoscales. This may impact various important climate processes, such as air-sea-ice fluxes of heat and carbon and rates of biological production, due to modifications in upper ocean stratification and circulation.

Our results have implications for understanding sea-ice formation, melt, and extent in the Southern Ocean. Numerical studies or observations in the Arctic (e.g., Lu et al., 2015) suggest that submesoscale processes enhance both the lateral and vertical heat transport by ~100 W m^{-2} each, which can buffer heat loss to the atmosphere and delay sea-ice onset (Su et al., 2018). Lateral freshwater transport can directly impact timing and magnitude of sea-ice formation or melting, while lateral stirring can impact sea-ice distribution (e.g., widening of the MIZ - Manucharyan & Thompson, 2017). Our observations show for the first time in the Southern Ocean the persistence (over several months) of lateral density gradients in the MIZ. This provides a continuous potential for submesoscale restratification (e.g., du Plessis et al., 2017), reducing the potential for mixing and thus ventilation of warm and carbon rich Circumpolar Deep Waters beneath the stratified winter water layer. We suggest future observational efforts (e.g., glider surveys, towed instruments), sampling at the appropriate time and space scales, should focus on the transition zone between open water and sea ice to further unravel the magnitude and scales of atmosphere-ocean processes at the edge of and under sea ice.

Acknowledgments
This work was supported by the following grants: Wallenberg Academy Fellowship (WAF 2015.0186), Swedish Research Council (VR 2019-04400), STINT-NRF Mobility Grant and NRF-SANAP (SNA170522231782), and AFT was supported by the Terrestrial Hazard Observations and Reporting (THOR) and ONR (N00014-19-1-2421). We thank Sea Technology Services (STS), SANAP, the captain and crew of the S.A. Agulhas II for their field-work/technical assistance. We thank David Peddie of Offshore Sensing AS for assistance with the Sailbuoy. S.S. is grateful to Geoff Shilling and Craig Lee (APL, University of Washington) for hosting the gliders on IOP and the technical advice provided. ERA5 data are generated using Copernicus Climate Change Service Information, available online (www.ecmwf.int/en/forecasts/datasets/archive-datasets/reanalysis-datasets/era5). Data are available online (ftp://roammiz.com via anonymous login).

References

Abernathey, R., Cerovecki, I., Holland, P., Newsom, E., Mazloff, M., & Talley, L. D. (2016). Water-mass transformation by sea ice in the upper branch of the Southern Ocean overturning. *Nature Geoscience*, *9*(8), 596–601. https://doi.org/10.1038/ngeo2749

Adams, K., MacKinnon, J., Lucas, A. J., Nash, J., Shroyer, E., & Farrar, J. T. (2019). Multi-platform observations of small-scale lateral mixed layer variability in the northern Bay of Bengal. *Deep Sea Research Part II*, *168*. https://doi.org/10.1016/j.dsr2.2019.07.017

Boccaletti, G., Ferrari, R., & Fox-Kemper, B. (2007). Mixed layer instabilities and restratification. *Journal of Physical Oceanography*, *37*, 2228–2250. https://doi.org/10.1175/JPO3101.1

Campbell, E. C., Wilson, E. A., Moore, G. W. K., Riser, S. C., Brayton, C. E., Mazloff, M. R., & Talley, L. D. (2019). Antarctic offshore polynyas linked to Southern Hemisphere climate anomalies. *Nature*, *570*(7761), 319–325. https://doi.org/10.1038/s41586-019-1294-0

du Plessis, M., Swart, S., Ansorge, I. J., & Mahadevan, A. (2017). Submesoscale processes accelerate seasonal restratification in the Subantarctic Ocean. *Journal of Geophysical Research*, *122*, 2960–2975. https://doi.org/10.1002/2016JC012494

du Plessis, M. D., Swart, S., Ansorge, I. J., Mahadevan, A., & Thompson, A. F. (2019). Southern Ocean seasonal restratification delayed by submesoscale wind-front interactions. *Journal of Physical Oceanography*, *49*(4), 1035–1053. https://doi.org/10.1175/JPO-D-18-0136.1

Ferrari, R., Paparella, F., Rudnick, D. L., & Young, W. R. (2001). The temperature-salinity relationship of themixed layer. In P. Müller & D. Henderson (Eds.), *Proceedings of the 12th 'Aha Huliko' a Hawaiian Winter Workshop* (pp. 95–104). Department of Oceanography, University of Hawaii (*From Stirring to Mixing in a Stratified Ocean*).

Fox-Kemper, B., Ferrari, R., & Hallberg, R. (2008). Parameterization of mixed layer Eddies. Part I: Theory and diagnosis. *Journal of Physical Oceanography*, *38*, 1145–1165. https://doi.org/10.1175/2007JPO3792.1

Ghani, M. H., Hole, L. R., Fer, I., Kourafalou, V. H., Wienders, N., Kang, H., et al. (2014). The Sailbuoy remotely-controlled unmanned vessel: Measurements of near surface temperature, salinity and oxygen concentration in the northern Gulf of Mexico. *Methods in Oceanography*, *10*, 104–121. https://doi.org/10.1016/j.mio.2014.08.001

Gruber, N., Landschützer, P., & Lovenduski, N. S. (2019). The variable Southern Ocean carbon sink. *Annual Review of Marine Science*, *11*(1), 159–186. https://doi.org/10.1146/annurev-marine-121916-063407

Horvat, C., Tziperman, E., & Campin, J.-M. (2016). Interaction of sea ice floe size, ocean eddies, and sea ice melting. *Geophysical Research Letters*, *43*, 8083–8090. https://doi.org/10.1002/2016GL069742

Hosegood, P., Gregg, M. C., & Alford, M. H. (2006). Sub-mesoscale lateral density structure in the oceanic surface mixed layer. *Geophysical Research Letters*, *33*, L22604. https://doi.org/10.1029/2006GL026797

Johnson, G. C., Schmidtko, S., & Lyman, J. M. (2012). Relative contributions of temperature and salinity to seasonal mixed layer density changes and horizontal density gradients. *Journal of Geophysical Research*, *117*, C04015. https://doi.org/10.1029/2011JC007651

Johnson, L., Lee, C. M., & D'Asaro, E. A. (2016). Global Estimates of Lateral Springtime Restratification. *Journal of Physical Oceanography*, *46*, 1555–1573. https://doi.org/10.1175/JPO-D-15-0163.1

Klein, P., & Lapeyre, G. (2009). The oceanic vertical pump induced by mesoscale and submesoscale turbulence. *Annual Review of Marine Science*, *1*(1), 351–375. https://doi.org/10.1146/annurev.marine.010908.163704

Lin, X., Zhai, X., Wang, Z., & Munday, D. R. (2018). Mean, variability, and trend of Southern Ocean wind stress: Role of wind fluctuations. *Journal of Climate*, *31*, 3557–3573. https://doi.org/10.1175/JCLI-D-17-0481.1

Lu, K., Weingartner, T., Danielson, S., Winsor, P., Dobbins, E., Martini, K., & Statscewich, H. (2015). Lateral mixing across ice meltwater fronts of the Chukchi Sea shelf. *Geophysical Research Letters*, *42*, 6754–6761. https://doi.org/10.1002/2015GL064967

Mahadevan, A., Tandon, A., & Ferrari, R. (2010). Rapid changes in mixed layer stratification driven by submesoscale instabilities and winds. *Journal of Geophysical Research*, *115*, C03017. https://doi.org/10.1029/2008JC005203

Manucharyan, G. E., & Thompson, A. F. (2017). Submesoscale Sea ice-ocean interactions in marginal ice zones. *Journal of Geophysical Research: Oceans*, *122*, 9455–9475. https://doi.org/10.1002/2017JC012895

Marshall, D. P., & Zanna, L. (2014). A conceptual model of ocean heat uptake under climate change. *Journal of Climate*, *27*(22), 8,444–8,465. https://doi.org/10.1175/JCLI-D-13-00344.1

Marshall, G. J. (2003). Trends in the Southern Annular Mode from observations and reanalyses. *Journal of Climate*, *16*, 4134–4143.

Massom, R. A., & Stammerjohn, S. E. (2010). Antarctic Sea ice change and variability—Physical and ecological implications. *Polar Science*, *4*(2), 149–186. https://doi.org/10.1016/j.polar.2010.05.001

Moran, M. D., & Pielke, R. A. (1994). Delayed shear enhancement in mesoscale atmospheric dispersion. United States. American Meteorological Society annual meeting, Nashville, TN (United States), 23-28 Jan 1994.

Pellichero, V., Sallée, J.-B., Schmidtko, S., Roquet, F., & Charrassin, J.-B. (2017). The ocean mixed layer under Southern Ocean sea-ice: Seasonal cycle and forcing. *Journal of Geophysical Research: Oceans*, *122*, 1608–1633. https://doi.org/10.1002/2016JC011970

Ramachandran, S., Tandon, A., Mackinnon, J., Lucas, A. J., Pinkel, R., Waterhouse, A. F., et al. (2018). Submesoscale processes at shallow salinity fronts in the Bay of Bengal: Observations during the winter monsoon. *Journal of Physical Oceanography*, *48*, 479–509. https://doi.org/10.1175/JPO-D-16-0283.1

Rudnick, D. L., & Ferrari, R. (1999). Compensation of horizontal temperature and salinity gradients in the ocean mixed layer. *Science*, *283*(5401), 526–529. https://doi.org/10.1126/science.283.5401.526

Schmidt, K. M., Swart, S., Reason, C., & Nicholson, S. -A. (2017). Evaluation of satellite and reanalysis wind products with in situ Wave Glider wind observations in the Southern Ocean. *Journal of Atmospheric and Oceanic Technology*, *34*(12), 2551–2568. https://doi.org/10.1175/JTECH-D-17-0079.1

Shroyer, E. L., Gordon, A. L., Jaeger, G. S., Freilich, M., Waterhouse, A. F., & Farrar, J. T. (2019). Upper layer thermohaline structure of the Bay of Bengal during the 2013 northeast monsoon. *Deep Sea Research Part II: Topical Studies in Oceanography*, 104630. https://doi.org/10.1016/j.dsr2.2019.07.018

Su, Z., Wang, J., Klein, P., Thompson, A. F., & Menemenlis, D. (2018). Ocean submesoscales as a key component of the global heat budget. *Nature Communications*, *9*(1), 775. https://doi.org/10.1038/s41467-018-02983-w

Swart, S., Gille, S. T., Delille, B., Josey, S., Mazloff, M., Newman, L., et al. (2019). Constraining Southern Ocean air-sea-ice fluxes through enhanced observations. *Frontiers in Marine Science*, *6*, 421. https://doi.org/10.3389/fmars.2019.00421

Swart, S., Thomalla, S. J., & Monteiro, P. M. S. (2015). The seasonal cycle of mixed layer characteristics and phytoplankton biomass in the Sub-Antarctic Zone: A high-resolution glider experiment. *Journal of Marine Systems*. https://doi.org/10.1016/j.jmarsys.2014.06.002

Thomas, L. N., & Ferrari, R. (2008). Friction, frontogenesis, and the stratification of the surface mixed layer. *Journal of Physical Oceanography*, *38*, 2501–2518.

Thomas, L. N., & Lee, C. M. (2005). Intensification of ocean fronts by down-front winds. *Journal of Physical Oceanography*, *35*, 1086–1102.

Thomas, L. N., Tandon, A., & Mahadevan, A. (2008). Submesoscale processes and dynamics. In *Ocean Modeling in an Eddying Regime*, *Geophys. Monogr.* (Vol. 177, pp. 17–38). Washington, DC: American Geophysical Union. https://doi.org/10.1029/177GM04

Thomas, L. N., Taylor, J. R., Ferrari, R., & Joyce, T. M. (2013). Symmetric instability in the Gulf Stream. *Deep Sea Research, Part II*, *91*, 96–110.

Thompson, A. F., Lazar, A., Buckingham, C., Naveira Garabato, A. C., Damerell, G. M., & Heywood, K. J. (2016). Open-ocean submesoscale motions: A full seasonal cycle of mixed layer instabilities from gliders. *Journal of Physical Oceanography*, *46*, 1285–1307. https://doi.org/10.1175/JPO-D-15-0170.1

Timmermans, M.-L., Cole, S., & Toole, J. (2012). Horizontal density structure and restratification of the Arctic Ocean surface layer. *Journal of Physical Oceanography*, *42*, 659–668.

Timmermans, M.-L., Toole, J., Proshutinsky, A., Krishfield, R., & Plueddemann, A. (2008). Eddies in the Canada Basin, Arctic Ocean, observed from ice-tethered profilers. *Journal of Physical Oceanography*, *38*, 133–145. https://doi.org/10.1175/2007JPO3782.1

Timmermans, M.-L., & Winsor, P. (2013). Scales of horizontal density structure in the Chukchi Sea surface layer. *Continental Shelf Research*, *52*, 39–45. https://doi.org/10.1016/j.csr.2012.10.015

Toole, J. M., Timmermans, M.-L., Perovich, D. K., Krisheld, R. A., Proshutinsky, A., & Richter-Menge, J. A. (2010). Influences of the ocean surface mixed layer and thermohaline stratification on Arctic Sea ice in the central Canada Basin. *Journal of Geophysical Research*, *115*, C10018. https://doi.org/10.1029/2009JC005660

von Appen, W.-J., Wekerle, C., Hehemann, L., Schourup-Kristensen, V., Konrad, C., & Iversen, M. H. (2018). Observations of a submesoscale cyclonic filament in the marginal ice zone. *Geophysical Research Letters*, *45*, 6141–6149. https://doi.org/10.1029/2018GL077897

Walin, G. (1982). On the relation between sea-surface heat flow and thermal circulation in the ocean. *Tellus*, *34*, 187–195. https://doi.org/10.1111/j.2153-3490.1982.tb01806.x

Wulff, T., Bauerfeind, E., & von Appen, W.-J. (2016). Physical and ecological processes at a moving ice edge in the Fram Strait as observed with an AUV. *Deep Sea Research*, *115*, 253–264. https://doi.org/10.1016/j.dsr.2016.07.001

Yuan, X. (2004). High-wind-speed evaluation in the Southern Ocean. *Journal of Geophysical Research*, *109*, D13101. https://doi.org/10.1029/2003JD004179